scientific reports

Check for updates

OPEN

Exploring the magnetohydrodynamic stretched flow of Williamson Maxwell nanofluid through porous matrix over a permeated sheet with bioconvection and activation energy

Sohaib Abdal[1], Imran Siddique[2], Dalal Alrowaili[3], Qasem Al-Mdallal[4]✉ & Sajjad Hussain[5]

The evolution of compact density heat gadgets demands effective thermal transportation. The notion of nanofluid plays active role for this requirements. A comparative account for Maxwell nanofluids and Williamson nanofluid is analyzed. The bioconvection of self motive microorganisms, non Fourier heat flux and activation energy are new aspects of this study. This article elaborates the effects of viscous dissipation, Cattaneo–Christov diffusion for Maxwell and Williamson nanofluid transportation that occurs due to porous stretching sheet. The higher order non-linear partial differential equations are solved by using similarity transformations and a new set of ordinary differential equations is formed. For numerical purpose, Runge–Kutta method with shooting technique is applied. Matlab plateform is used for computational procedure. The graphs for various profiles .i.e. velocity, temperature, concentration and concentration of motile micro-organisms are revealed for specific non-dimensional parameters. It is observed that enhancing the magnetic parameter *M*, the velocity of fluid decreases but opposite behavior happens for temperature, concentration and motile density profile. Also the motile density profile decrease down for *Pe* and *Lb*. The skin friction coefficient is enhanced for both the Williamson and Maxwell fluid.

Nomenclature

Latin symbols

u, v	Velocity components
(x,y)	Cartesian coordinates
u_w	Velocity of the fluid at wall
n	Power law index
B_o	Magnetic field strength
C	Concentration of nanoparticles
T	Temperature of nanoparticles
N	Micro-rotation vector
k^*	Mean absorption co-efficient
k_1	Permeability of porous medium
k	Fluid parameter

[1]Northwest University, School of Mathematics, Xian 7100069, China. [2]Department of Mathematics, University of Management and Technology, Lahore 54770, Pakistan. [3]Department of Mathematics, College of Science, Jouf University, Sakaka 2014, Saudi Arabia. [4]Department of Mathematics Sciences, UAE University, Al Ain 15551, United Arab Emirates. [5]School of Aerospace and Mechanical Engineering, Nanyang Technological University, Singapore, Singapore. ✉email: q.almdallal@uaeu.ac.ae

C_p	Specific heat at constant pressure
τ_1, τ_2	Relaxation time of heat flux
D_B	Brownian diffusion constant
D_T	Thermophoresis diffusion coefficient
T_∞	Free stream temperature
C_∞	Free stream concentration of nanoparticles
Q_1	Heat source/sink coefficient
M	Magnetic field parameter
K	Micropolar parameter
Kp	Porosity parameter
t	Time
Pr	Prandtl number
R	Thermal radiation parameter
Nb	Brownian motion parameter
Nt	Thermophoresis parameter
Sc	Schmidt number
Q'	Heat source parameter
T_w	Wall constant temperature
C_w	Nanoparticles concentration at wall
W_e	Local Weissenberg number
f	Dimensionless stream function
C_f	Skin friction coefficient
Sh_x	Sherwood number
Nu_x	Nusselt number
Re_x	Local Reynolds

Greek symbols

α	Thermal diffusivity of base fluid
μ	Viscosity of fluid
ψ	Stream function
ν	Kinematic viscosity
σ	Electrical conductivity
σ^*	Stefan–Boltzmann constant
ρ	Density of fluid
ρ_p	Nanoparticle's density
γ	Spin gradient viscosity
γ_1	Thermal relaxation parameter
γ_2	Solutal relaxation parameter
η	Similarity variable
θ	Similarity temperature
ϕ	Similarity concentration of nanoparticles
Γ	Material time constant
δ	Unsteadiness parameter

Subscripts

p	Nanoparticles
w	On the accelerated surface
∞	Free stream

In modelling of fluids flows with shear-dependent viscosity, the power-law model is commonly used. But the consequences of elasticity are impossible to be anticipated. The results of elasticity can be achieved by second grade or third grade fluids. But the viscosity is not shear-dependent in these models. In addition, they are unable to determine the impacts of calming stress. A subdivision of fluids of the rate form, viz., Maxwell model can predict stress relaxation and has thus become more common. As in the Maxwell model, a strictly viscous damper and a purely elastic spring can be described. Many researchers have pondered Maxwell nanofluid flow simulations. Maxwell nanofluids with normal kernel through fractional derivatives studded by Abro et al.[1]. Numerical analysis of Maxwell nanofluid flows past a linearly stretched layer was reviewed by Sharama et al.[2]. Assessment of bioconvection in Maxwell nanofluid configured with nonlinear thermal radiation and activation energy using a Riga surface was conducted by Ramesh et al.[3]. Ahmed et al.[4] reviewed the impact of radiative heat flux in Maxwell nanofluid flow over a chemically reacted spiralling disc. Mathematical analysis of Maxwell nanofluid with hydromagnetic dissipative and radiation was considered by Hussain et al.[5]. Jawad et al.[6] calculated the entropy generation for magnetohydrodynamic (MHD) mixed convection and Maxwell nano-fluid flow over an elongating and penetrable surface in the presence of heat conductivity, velocity slip boundary condition and thermal radiation.

English scientist Williamson presented the Williamson model[7] in 1929 and several other researchers studied it. Williamson fluid has a shear thinning property typical of a non-Newtonian fluid model. Later, perturbation solution of incompressible flows in a rock fracturing with a non-Newtonian Williamson fluid was studied by

Dapra et al.[8]. Nadeem et al.[9] studded Wiliamson nanofluid stream on an extended sheet in twenty first century. Even now in 2020, several scholar are rivaling the properties of Williamson nano-fluid such as, analysis of gyrotactic microorganisms with activation energy in the radiated liquid was provoked Haq et al.[10]. The impact of the magnetic field in a curved channel on the peristaltic flow of Williamson fluid was explored by Rashid et al.[11]. Habib et al.[12] carried out a comparison research on micropolar, Williamson, and Maxwell nanofluids flow owing to a stretched surface in the presence of bioconvection and double diffusion along the activation energy. Waqas et al.[13] conducted research for the generalized principle of Fourier and Fick to effect Williamson fluid flow. Analysis of heat transfer for electro-osmotic stream across of the micro-channel for Williamson fluid motion was discussed by Noreen et al.[14].

Hydrodynamic volatility and patterns in suspensions of biased swimming microorganisms are characterized by the term bio-convection. In the early 21st century, biotechnology has developed to incorporate modern and complex disciplines. Bioconvection has various uses in natural systems and biotechnology. Various researchers commit their resources to reveal the characteristics of bio-convection. Bioconvection has various uses in natural systems and biotechnology. Numerical study of bio-convective nanofluid on a magnetohydrodynamic slip flow with stephan blowing was considered by Tuz et al.[15]. The effects of energy on Eyring nanofluid flow containing motile microorganism was studied by Sharief et al.[16]. Sharma et al.[17] adopted non-dimensional measurements to examine the effect of heat and mass flux on the natural convective laminar movement of a viscoelastic immiscible fluid. Sharma et al.[18] studied the impacts of a chemical change and a heat source on magneto-hydrodynamic assorted convective mass and heat transfer flow over a vertical plate. For a Casson nanofluid stream over a stretching/shrinking sheet, magagula et al.[19] tested the influence of an applicable magnetic field, nonlinear thermal radiation and first-order chemical reaction double dispensed bioconvection. Shaw et al.[20] presented a homogeneous model for oxytactic microbial bioconvection in a non-Darcy permeable material. Khan et al.[21] studied the impacts of Arrhenius activation energy, binary chemical reaction and viscous dissipation on the bioconvective micropolar flow of nanofluid over a slim moving needle containing gyrotactic micro-organisms.

A highly promising nanostructure analysis was primarily conducted by Choi et al.[22] to show that the presence of nanoparticles in base fluids can be beneficial in improving the rheological effects of typical base fluids. "Nanofluid is a suspension comprising nanoparticles in a base liquid (water, base fluid mixture, kerosene, biofluids and organic liquids) that alters the viscosity, thermal conductivity, density, and mass diffusivity of the base fluid".In the last few decades, companies have evolved to research fluid mechanics on the nano and micro scales. For improved oil recovery in a heterogeneous two-dimensional anticline geometry, nanofluid flooding investigated by Esfe et al.[23]. Khader et al.[24]utilized the fourth order predictor-corrector finite difference technique to analyse the influence of thermal radiation and a non-uniform heat source on unsteady MHD micropolar fluid flow past a stretching sheet. Verma et al.[25] examined the steady two-dimensional, laminar, viscous and incompressible boundary layer movement of $Cu/Ag - H_2O$ nanoparticles. kumaran et al.[26] employed the Keller box technique to examine the effect of thermal conductivity variation and thermal radiation on chemically reacting and free convective Powell-Eyring nanofluid flow across a cylinder. Sharma et al.[27] explored an irregular magneto-hydrodynamic (MHD) natural convection transmission of mass and thermal over a porous medium sheet under the impact of thermal radiation and thermo-diffusion consequences using the Laplace transform tactic. Jena et al.[28] numerically investigated nanofluid stream transmission through permeable media with a heat source/sink and a chemical process. Nayak et al.[29] discussed slip consequences of the flow of chemically reactive Casson nanofluid flowing over an exponentially stretched electromagnetic sheet. Saranya et al.[30] researched the two-dimensional consistent convective boundary layer fluid motion and heat transmit of Newtonian/non-Newtonian base liquids with magnetic nanoparticles over a flat plate with non-linear thermal radiation and slip implications. Kairi et al.[31] assumed that the bioconvection of Casson nanoparticles over an inclined elongating sheet. Sharma et al.[32] exploited the perturbation approach to analyse the electrically conducting fluid motion over a vertical plane sheet. The diverse applications of nanofluids in various aspects are examined by some other scholars[33–36].

In1942, Hannes Alfvén made the first recorded use of the term "Magnetohydrodynamics".It originated from the magneto-meaning magnetic field, hydro-meaning water, and dynamics-meaning motion. MHD is utilized in divers fields of engineering, industrial and mostly in the nanotech field. All around the globe, scholars are devoting their time and efforts to reveal the characteristics. In recent time, many scholars worked on the properties of MHD as discussed Rasool et al.[37]. Ahmad et al.[38] applied the homotopy analysis method (HAM) to examine the fluid film flow of an Oldroyd-B fluid past a spinning disc in three-dimensional space under the implications of heat absorption/omission and radiation terminologies. Gul et al.[39] employed the RK-4 method to investigate the MHD (magneto-hydrodynamics) unsteady and immiscible flow of nanofluid flow caused by a stretching rotating disc with the effect of Joule heating and dispersion. Gul et al.[40] investigated the 3-D Darcy-Forchheimer MHD Casson fluid and steady flow between the difference between a disc and a cone in a rotating strategy in the presence of thermal diffusion effect and Brownian movement[41,42] scrutinized the MHD flow attributes in distinct aspects.

The impact of bioconvection of micro-organism for two different flows of Williamson nanofluid and Maxwell nanofluid is rarely studied in the existing literature. It helps to cope with the possible settling of nano-entities and thus improvement of thermal conductivity of the common fluids can be established. The novelty of this work pertains to Cattaneo–Christov heat flux, bioconvection and activation energy. The buoyancy effects, magnetic field strength imparts differentiated influence on flow temperature and concentration characteristics. The role of these useful and practicable physical aspects for two significant non-Newtonian fluids is enumerated and their comparative outcomes help to broaden our understanding and utilization of these flows. By utilization of similarity transforms enable to yield numerical solution of non-linear coupled system with the implementation of Runge–Kutta method and shooting technique. By utilizing the parametric evolution of bioconvection, nanofluid slips and Cattaneo–Christov factor, the findings are evaluated for Maxwell fluid and Williamson fluid. These results are beneficial for thermal management of heat exchangers of the emerging technologies.

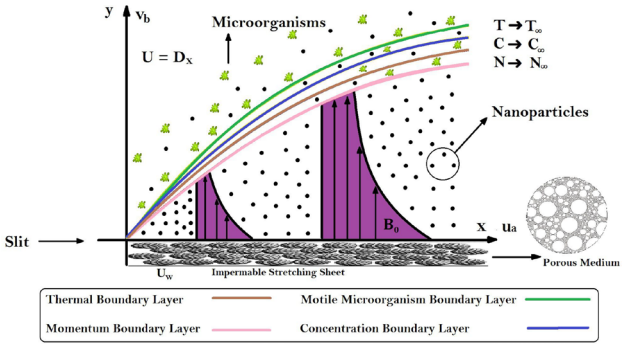

Figure 1. Problem description.

Physical model and mathematical formulation

A two-dimensional, steady flow of Maxwell and Williamson nanofluid with activation energy and Cattaneo–Christov diffusion embedded in a porous medium is discussed in the existence of bioconvection of microorganisms. The fluids flow owing to a stretching sheet, The wall velocity is $U_w = Dx$, D is stretching constant. U_w is the stretching velocity of sheet along x-axis. It is assumed that behavior of the flow is linear due to the impermeable stretching sheet. Here u_a and v_b are the velocities of fluids flow along x-axis and y-axis. In Fig. 1, the temperature of fluids, concentration and density of microorganisms near the sheet are taken as T, C, and N. Now our problem represents the basic equations of continuity, equation of momentum, energy equation, concentration equation and gyrotactic microorganism's concentration equation in Cartesian coordinates.

The following equation are established in the aspects of flow of fluids. The governing equations for the problems are given below[5,8,16]:

$$\frac{\partial u_a}{\partial x} + \frac{\partial v_b}{\partial y} = 0, \tag{1}$$

$$u_a\frac{\partial u_a}{\partial x} + v_b\frac{\partial u_a}{\partial y} = \nu\frac{\partial^2 u_a}{\partial y^2} + \sqrt{2}\nu\Gamma\frac{\partial u_a}{\partial y}\frac{\partial^2 u_a}{\partial y^2} - \frac{\sigma B_0^2 u_a}{\rho} - \frac{\nu}{k'}u_a - \lambda_1\left[u_a^2\frac{\partial^2 u_a}{\partial x^2} + v_b^2\frac{\partial^2 u_a}{\partial y^2} + 2u_a v_b\frac{\partial^2 u_a}{\partial y \partial x}\right] + \left(\frac{1}{\rho}\right)\left((1-C_\infty)\rho\beta(T-T_\infty) - (\rho_p-\rho)g(C-C_\infty) - (N-N_\infty)g\gamma(\rho_m-\rho)\right), \tag{2}$$

$$u_a\frac{\partial T}{\partial x} + v_b\frac{\partial T}{\partial y} = \alpha\frac{\partial^2 T}{\partial y^2} + \frac{\rho_p C_p}{\rho C}\left[D_B\frac{\partial C}{\partial y}\frac{\partial T}{\partial y} + \frac{D_T}{T_\infty}\left(\frac{\partial T}{\partial y}\right)^2\right] + \tau_1\left[u_a\frac{\partial u_a}{\partial x}\frac{\partial T}{\partial x} + v_b\frac{\partial v_b}{\partial x}\frac{\partial T}{\partial x} + u_a\frac{\partial v_b}{\partial x}\frac{\partial T}{\partial x} + v_b\frac{\partial u_a}{\partial y}\frac{\partial T}{\partial x} + 2u_a v_b\frac{\partial^2 T}{\partial x \partial y} + u_a^2\frac{\partial}{\partial x}\frac{\partial T}{\partial x} + v_b^2\frac{\partial}{\partial y}\frac{\partial T}{\partial y}\right], \tag{3}$$

$$u_a\frac{\partial C}{\partial x} + v_b\frac{\partial C}{\partial y} = D_B\frac{\partial}{\partial y}\frac{\partial C}{\partial y} + \frac{D_T}{T_\infty}\frac{\partial}{\partial y}\frac{\partial T}{\partial y} - (Kr)^2(C_w - C_\infty)\left(\frac{T}{T_\infty}\right)^m exp\left(\frac{-E_a}{k_2 T}\right), \tag{4}$$

$$u_a\frac{\partial N}{\partial x} + v_b\frac{\partial N}{\partial y} + bW_c\frac{\partial}{\partial y}\left(\frac{n}{\Delta C}\frac{\partial C}{\partial y}\right) = D_m\frac{\partial}{\partial y}\frac{\partial N}{\partial y}. \tag{5}$$

$$\left.\begin{aligned} u_a = U_w = Dx, v_b = v_w, T - T_w(x) = 0, C - C_w(x) = 0, N - N_w(x) = 0, \quad at \quad y = 0, \\ u_a \to 0, \quad T \to T_\infty, \quad C \to C_\infty, \quad N \to N_\infty \quad as \quad y \to \infty. \end{aligned}\right\} \tag{6}$$

Using the similarity variables:

$$\left.\begin{aligned} \eta = \sqrt{\frac{D}{\nu}}y,\ u_a = Dxf'(\eta), v_b = -\sqrt{D\nu}f(\eta), \theta(\eta) = \frac{T-T_\infty}{T_w-T_\infty}, \\ \phi(\eta) = \frac{C-C_\infty}{C_w-C_\infty}, \chi(\eta) = \frac{N-N_\infty}{N_w-N_\infty} \end{aligned}\right\} \tag{7}$$

where we have λ_1 is fluid relaxation time, Γ is Williamson fluid parameter. It is to mentioned that in Eq. (2) when $\lambda_1 = 0$ and $\Gamma \neq 0$, it is Williamson fluid flow. Also for $\Gamma = 0$ and $\lambda_1 \neq 0$, than it is Maxwell fluid flow. Equation (1) is balanced identically. Equations (2) to (5) are rescaled as below:

$$f''' - f'^2 + ff'' - \beta(f^2 f''' - 2ff'f'') + \lambda f''f''' - (M + K_p)f' + \omega(\theta - Nr\phi - Rb\chi) = 0, \tag{8}$$

$$\theta'' + Prf\theta' + \frac{Nc}{Le}\theta'\phi' + \frac{Nc}{Le * Nbt}\theta'^2 + b(f^2\theta'' + ff'\theta') = 0, \tag{9}$$

$$\phi'' + Sc(f\phi') + \left(\frac{1}{Nbt}\right)\theta'' - Sc * A\phi(1+\delta\theta)^m \exp\left(\frac{-E}{1+\delta\theta}\right) = 0, \tag{10}$$

$$\chi'' + Lb(f\chi') - Pe[\phi''(\chi+\Omega) + \chi'\phi'] = 0. \tag{11}$$

$$\left.\begin{aligned} f(0) = S,\ f'(0) = 1,\ \theta(0) = 1,\ \phi(0) = 1,\ \chi(0) = 1,\ at\ \eta = 0, \\ f'(\infty) \to 0,\ \theta(\infty) \to 0, \phi(\infty) \to 0, \chi(\infty) \to 0,\ as\ \eta \to \infty. \end{aligned}\right\} \tag{12}$$

The non-dimensional parameters in their respective order:

β, λ M, Kp, ω, Nr, Rb, Rd, Pr, Le, Nbt, b, Q, Sc, A, δ, E, Lb, Pe, Ω, and S are Deborah number, non-newtonian Williamson parameter, magnetic parameter, porosity parameter, mixed convection, buoyancy ratio, Rayleigh number, radiation, Prandtl number, Lewis number, diffusivity ratio, thermal relaxation constant, heat source, Schimdt number, dimensionless reaction rate, temperature difference, activation energy, bio-convection Lewis number, bio-convection Peclet number, microorganism concentration difference, suction/injection parameter.

Where: $\beta = \lambda_1 D$. $M = \frac{\sigma B_0^2}{D\rho}$, $Kp = \frac{\nu}{k_1 D}$, $\omega = \frac{\beta_1 g(1-C_\infty)(T_w - T_\infty)}{D^2 x}$, $Nr = \frac{(\rho_p - \rho)(C_w - C_\infty)}{\beta_1 \rho(1-C_\infty)(T_w - T_\infty)}$, $Rb = \frac{(\rho_m - \rho)\gamma N_\infty}{(1-C_\infty)\rho\beta T_\infty}$, $Rd = \frac{16T_\infty^3 \sigma^*}{3k^*\kappa}$, $Pr = \frac{\nu}{\alpha}$, $Le = \frac{\alpha}{D_B}$, $Nbt = \frac{D_B T_\infty (C_w - C_\infty)}{D_T (T_w - T_\infty)}$, $b = \tau_1 D$, $Sc = \frac{\nu}{D_B}$, $A = \frac{k^2 r}{D}$, $\delta = \frac{T_w - T_\infty}{T_\infty}$, $E = \frac{E_a}{k_2 T_\infty}$, $Lb = \frac{\nu}{D_m}$, $Pe = \frac{b_1 Wc}{D_m}$, $\Omega = \frac{N_\infty}{N_w - N_\infty}$, $S = \frac{-v_w}{\sqrt{D\nu}}$.

The physical quantities are stated as[43]:

Cf_x (skin friction coefficient), Nu_x (local Nusselt number), Sh_x (local Sherwood number) and Nn_x (local density of microorganism) are given below:

$$\left.\begin{aligned} Cf_x = \frac{\tau_w}{\rho U^2 w},\ Nu_x = \frac{xq_w}{k(T_w - T_\infty)}, \\ Sh_x = \frac{xq_m}{D_B(C_w - C_\infty)},\ Nn_x = \frac{xq_n}{D_m(N_w - N_\infty)}. \end{aligned}\right\} \tag{13}$$

where τ_w, q_w, q_m and q_n denotes shear stress, surface heat flux, surface mass flux and motile microorganism flux are given by (at $y = 0$),

$$\left.\begin{aligned} \tau_w = \mu(1+\beta)(1 + \frac{\Gamma}{2}\frac{\partial u_a}{\partial y})\frac{\partial u_a}{\partial y},\ q_w = -K\frac{\partial T}{\partial y}, \\ q_m = -D_B\frac{\partial C}{\partial y},\ q_n = -D_m\frac{\partial N}{\partial y}. \end{aligned}\right\} \tag{14}$$

On solving these quantities with the help of given similarity transformation, we obtain:

$$\left.\begin{aligned} C_f(Re_x)^{-1/2} = (1+\beta)(f''(0) + \frac{\lambda}{2}f''(0)^2),\ Nu_x(Re_x)^{-1/2} = -\theta'(0), \\ Sh_x(Re_x)^{-1/2} = -\phi'(0),\ Nn_x(Re_x)^{-1/2} = -\chi'(0). \end{aligned}\right\} \tag{15}$$

where, $(Re_x) = \frac{xU_w}{\nu}$ is the local Reynolds number.

Solution procedure

For numerical results, nonlinear ordinary differential Equations (8) to (11) with the given boundary conditions Eq. (12) are solved by Runge–Kutta method of order four along with shooting technique. To execute this numerical method, the new variable expressed as below[44–46]:

$$\left.\begin{aligned} s_1' &= s_2 \\ s_2' &= s_3 \\ s_3' &= s_2^2 - s_1 s_3 + \beta(s_1^2 ds_3 - 2s_1 s_2 s_3) - \lambda s_3 ds_3 + (M + Kp)s_2 - \omega(s_4 - Nrs_6 - Rbs_8) \\ s_4' &= s_5 \\ s_5' &= -Prs_1 s_5 - \frac{Nc}{Le}s_5 s_7 - \frac{Nc}{Le * Nbt}s_5^2 - b(s_1^2 ds_5 + s_1 s_2 s_5) \\ s_6' &= s_7 \\ s_7' &= -Scs_1 s_7 - \frac{1}{Nbt}ds_5 + Sc * A[1 + \delta s_6]^n exp[\frac{-E}{1+\delta s_6}]s_8 \\ s_8' &= s_9 \\ s_9' &= -Lbs_1 s_9 + Pe[s_7 s_9 + (\Omega + s_8)ds_7] \end{aligned}\right\} \tag{16}$$

Pr	Nadeem et al.[48]	Khan and Pop[49]	Golra and Sidawi[50]	Present results
0.07	0.066	0.066	0.066	0.065
0.2	0.169	0.169	0.169	0.167
0.7	0.454	0.454	0.454	0.435
2.0	0.911	0.911	0.911	0.910

Table 1. The comparative outputs for $-\theta'(0)$.

M	*Kp*	ω	*Nr*	*Rb*	Maxwell fluid $\beta = 0.5$	Williamson fluid $\lambda = 0.1$
0.1	0.1	0.1	0.1	0.1	2.5113	1.2342
0.3					2.6257	1.3090
0.5					2.7341	1.3796
0.5	0.2				2.5693	1.2722
	0.4				2.6806	1.3448
	0.5				2.7341	1.3796
	0.5	0.1			2.7341	1.3796
		0.2			2.6512	1.3339
		0.3			2.5712	1.2897
		0.1	0.1		2.7341	1.3796
			0.2		2.7407	1.3834
			0.3		2.7474	1.3873
			0.1	0.1	2.7341	1.3796
				0.2	2.7389	1.3824
				0.3	2.7438	1.3852

Table 2. Results for $-f''(0)$.

Pr	*Nc*	*Nbt*	*b*	Maxwell fluid $\beta = 0.5$	Williamson fluid $\lambda = 0.1$
0.71	0.5	2.0	0.5	0.4045	0.4418
1.0				0.5237	0.5680
1.5				0.7129	0.7639
0.71	0.1			0.4439	0.4843
	0.5			0.4045	0.4418
	1.0			0.3598	0.3934
	0.5	1.0		0.3942	0.4306
		2.0		0.4045	0.4418
		3.0		0.4081	0.4456
		2.0	0.1	0.3769	0.4063
			0.3	0.3905	0.4238
			0.5	0.4045	0.4418

Table 3. Results for $-\theta'(0)$.

along with the boundary conditions[47]:

$$\left.\begin{aligned} s_1 = S,\ s_2 = 1,\ s_4 = 1,\ s_6 = 1,\ s_8 = 1, at\ \eta = 0, \\ s_2 \to 0,\ s_4 \to 0,\ s_6 \to 0,\ s_8 \to 0\ as\ \eta \to \infty. \end{aligned}\right\} \tag{17}$$

Results and discussions

In this part, we presented and explained the outcomes as computed from the above mentioned procedure. The validation of current results is established when these are compared with the existing findings of[48–50] in limiting cases.The four sets of results are contained in Table 1 and a close agreement is seen among them. Table 2 indicates that the drag force is supplemented with incremental variation of M, K_p. Nr, Rb in case of Maxwell fluid ($\beta = 0.5$) as well as Williamson fluid ($\lambda = 0.1$) and hence the magnitude of $-f''(0)$ (skin friction factor) is enhanced because of the additional resistance to the flow that comes into play with enhancement of magnetic parameters. However, the skin friction is reciprocated against mixed convection parameter ω, because the rise

Sc	*A*	δ	*E*	n	Maxwell fluid $\beta = 0.5$	Williamson fluid $\lambda = 0.1$
1.0	0.1	0.1	0.3	0.5	0.7333	0.7408
2.0					1.0157	1.0395
3.0					1.2887	1.3218
2.0	0.1				1.0157	1.0395
	0.2				1.1912	1.2084
	0.3				1.3389	1.3526
	0.1	0.1			1.0157	1.0395
		0.2			1.0261	1.0493
		0.3			1.0359	1.0586
		0.1	0.1		1.0546	1.0767
			0.3		1.0157	1.0395
			0.5		0.9818	1.0073
			0.3	0.1	1.0101	1.0342
				0.3	1.0129	1.0369
				0.5	1.0157	1.0395

Table 4. Results for $-\phi'(0)$.

Lb	*Pe*	Ω	Maxwell fluid $\beta = 0.5$	Williamson fluid $\lambda = 0.1$
0.4	1.2	0.2	1.6319	1.6748
0.8			1.7782	1.8269
1.2			1.9140	1.9662
1.2	0.4		1.0467	1.0892
	0.8		1.4761	1.5228
	1.2		1.9140	1.9662
	1.2	0.1	1.8102	1.8621
		0.2	1.9140	1.9662
		0.3	2.0178	2.0704

Table 5. Results for $-\chi'(0)$.

in mixed convection helps to accelerate the flow. Further, it is seen that the absolute value of $-f''(0)$ is larger for Maxwell nanofluid than that of Williamson nanofluid. Table 3 shows that Nusselt number $-\theta'(0)$ improves in direct relation to *Pr*, *Nbt* and *b*, but it diminishes against *Nc*. Table 4 convinced that $-\phi'(0)$ recedes only when *E* rises, while $-\phi'(0)$ is upsurged directly with *Sc*, *A*, δ and *n*. From Table 5, it is noticed that magnitude of motile density $-\chi'(0)$ is increased when *Lb*, *Pe* and Ω are uplifted. Also, it is observed that Maxwell nanofluid takes larger values than that of Williamson nanofluid for Nusselt number $-\theta'(0)$, $-\phi'(0)$ and for motile density $-\chi'(0)$.

Figure 2a explains the effect of magnetic field *M* on velocity profile $f'(\eta)$ for Maxwell and Williamson fluids. A reduction is produced in the boundary layer thickness by increasing the value of *M*. It is observed that Williamson fluid is highly affected as compared to the Maxwell fluids. Physically, the magnetic field has ability to enhance the drag force which is said as Lorentz force. This force prevents the fluid from flowing as well as causes an increment in the thickness of boundary layer. From Fig. 2b, it is seen that the enhanced porosity parameter K_p retards the flow velocity. Because K_p has ability to produce resistance for fluid flow. Mixed convection parameter effect on $f'(\eta)$ for Williamson and Maxwell nanofluids is discussed in Fig. 3a. The greater values of mixed convection parameter ω causes an increment in $f'(\eta)$ due to the larger buoyancy force. Figure 3b and c both explain the aspects of (*Rb*) bioconvection Rayleigh number as well as (*Nr*) buoyancy ratio parameter on $f'(\eta)$. The changing values of both the parameters cause decline in velocity distribution significantly. Physically, both parameters show their relation with buoyancy ratio forces which causes resistance in the motion of the two fluids. Moreover, the velocity for Williamson nanofluids is faster than that of Maxwell nanofluids. It means Maxwell fluid imparts more viscus effects on the flow than the Williamson fluid. The impacts of magnetic parameter *M* and Cattaneo-Christov parameter *b* on temperature profile $\theta(\eta)$ are illustrated in Fig. 4. Physically, *M* has the ability to intensify the temperature distribution profile due to the involvement of Lorentz force. Moreover by increasing the Cattaneo-Christov parameter *b* causes a reduction in $\theta(\eta)$. Thus Maxwell fluid diffuses more heat as compared to Williamson fluid and hence the temperature curve for Maxwell fluid is elevated than that of Williamson fluid. As it is clear that λ is a ratio between buoyancy forces to viscous force. Due to which a little change in λ causes a decrement in the $\theta(\eta)$. The impact of Lewis number *Le* on $\theta(\eta)$ is depicted in Fig. 5a. Depreciation in temperature profile is due to its direct relation with diffusivity of mass which causes reduction in the temperature distribution. The effect of *Pr* can be visualized on temperature profile in Fig. 5b. It is clear that by increasing the values of *Pr* causes a reduction in $\theta(\eta)$. Physically, it is due to the reverse relation of *Pr* with the thermal diffusivity. Fig. 5c explains the effect of *Nc* on temperature distribution, an increment in *Nc*

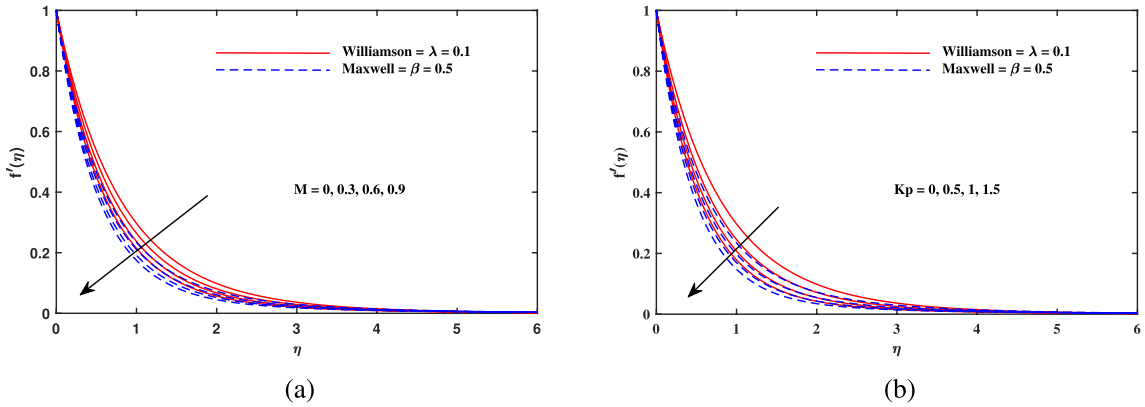

Figure 2. Velocity $f'(\eta)$ fluctuation with (**a**) M and (**b**) K_p.

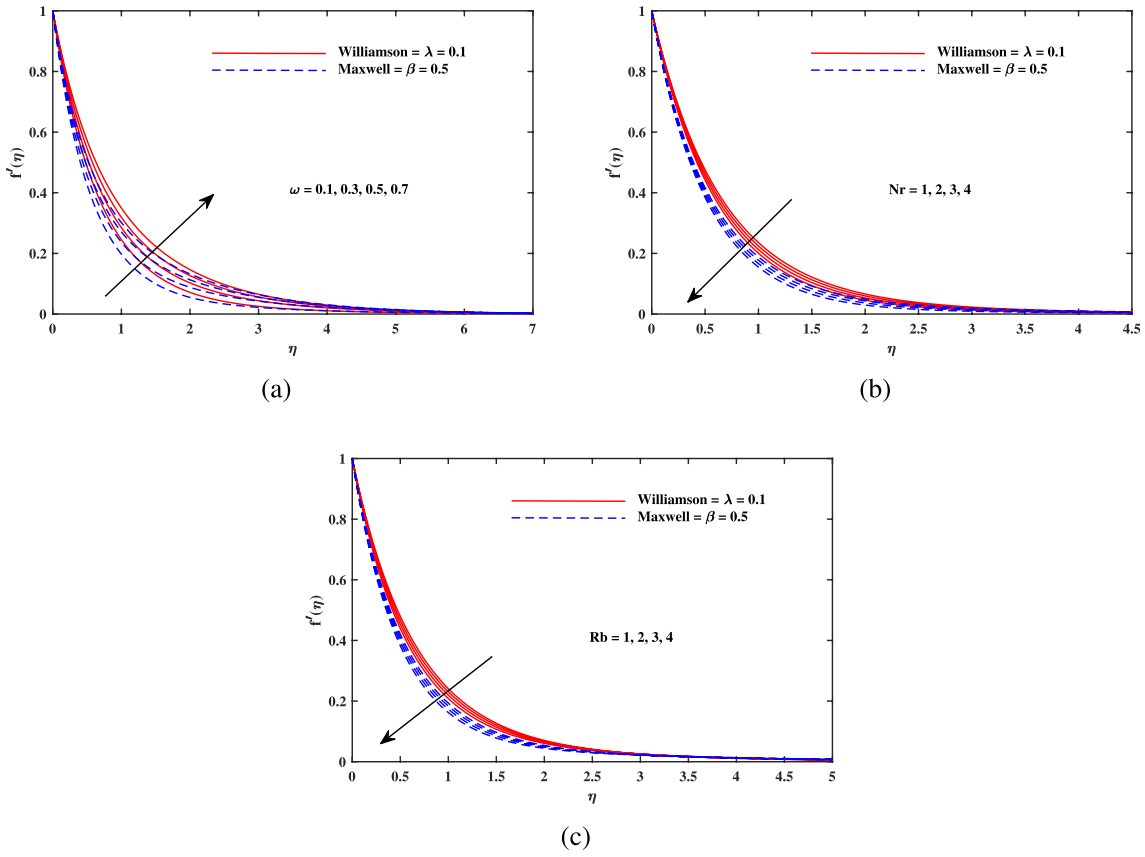

Figure 3. Velocity $f'(\eta)$ fluctuation with (**a**) ω, (**b**) Nr and (**c**) Rb.

causes an accession in temperature distribution. From Fig. 6, it can be visualized that increment in the magnetic number M as well as activation energy E causes an accession in the concentration profile $\phi(\eta)$. Increment in M causes an increase in Lorentz force which causes more resistance to the flow of Williamson fluid as compared to Maxwell fluid. A decrease in concentration profile $\phi(\eta)$ can be observed in Fig. 7 with the exceeding of chemical reaction rate parameter A as well as Lewis number Le. The larger inputs of A means faster chemical reaction to decline the concentration function $\phi(\eta)$. Similarly, higher Lewis number Le causes depreciation in $\phi(\eta)$ because it is related reciprocally to mass diffusivity. While the increment in A generates more resistance in Williamson fluid flow as compared to Maxwell fluids. Moreover decrement in mass diffusivity becomes Williamson fluid less resistive as compared to Maxwell fluid for flow. The motile density profile $\chi(\eta)$ is increased with the increment in M. It is due to slowing of flow. The curves generated by M results an accession in the motile density profile $\chi(\eta)$. It also shows an accession in it by increasing the value of microorganism difference parameter Ω which can be observed in Fig. 8. Figure 9 is drawn to discuss the results of Lewis number Lb as well as Peclet number Pe. The diffusivity of microorganisms is related with Peclet number Pe, which means greater value of Peclet number

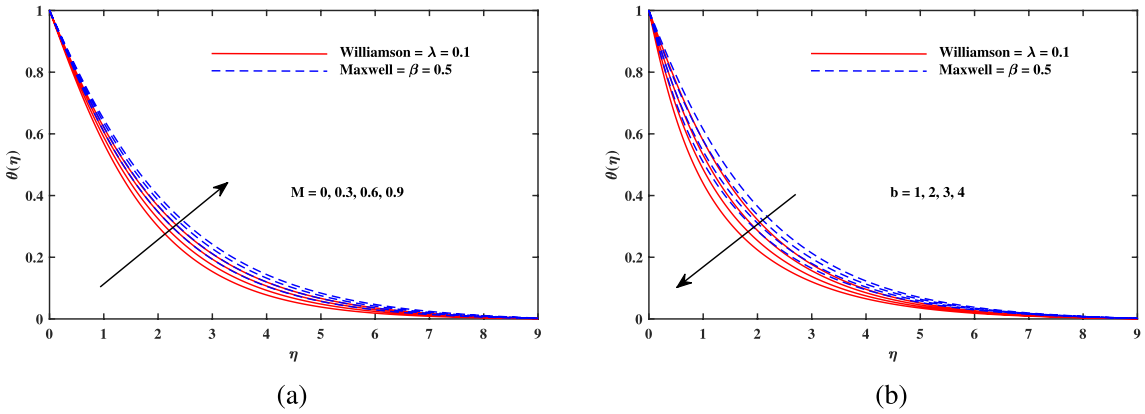

Figure 4. Temperature $\theta(\eta)$ fluctuation with of (**a**) M and (**b**) b.

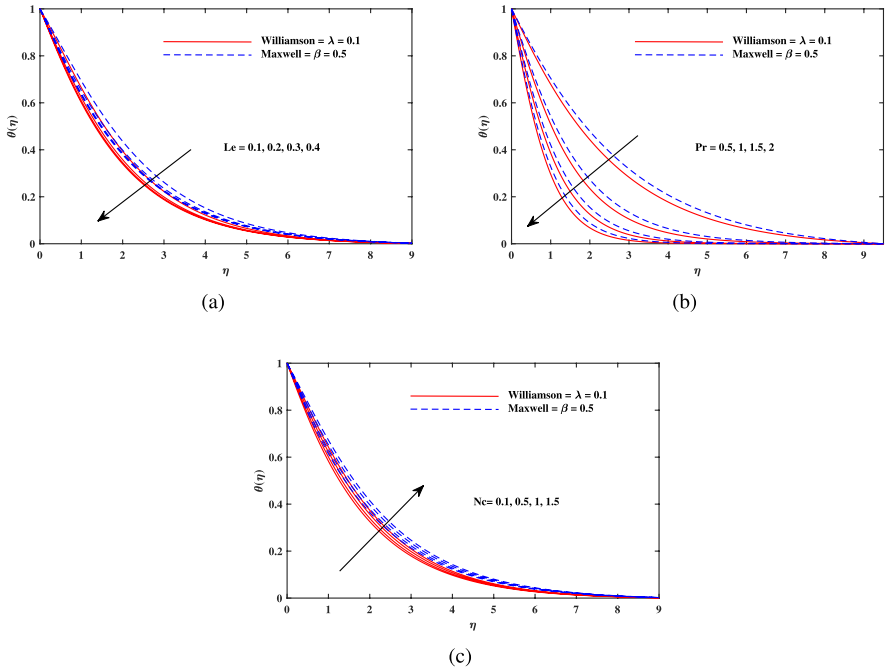

Figure 5. Temperature $\theta(\eta)$ fluctuation with (**a**) Le, (**b**) Pr and (**c**) Pr.

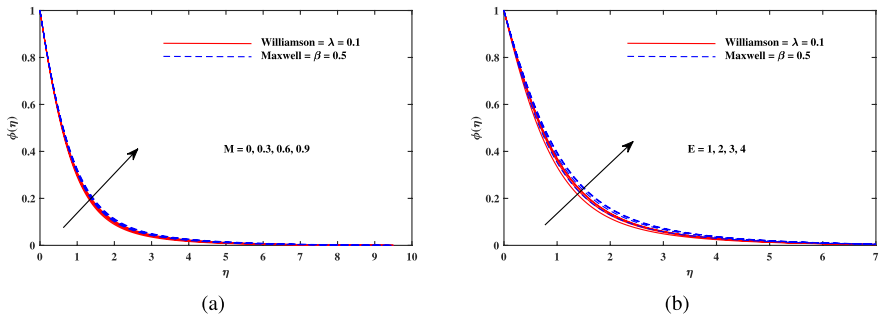

Figure 6. Concentration $\phi(\eta)$ fluctuation with (**a**) M and (**b**) E.

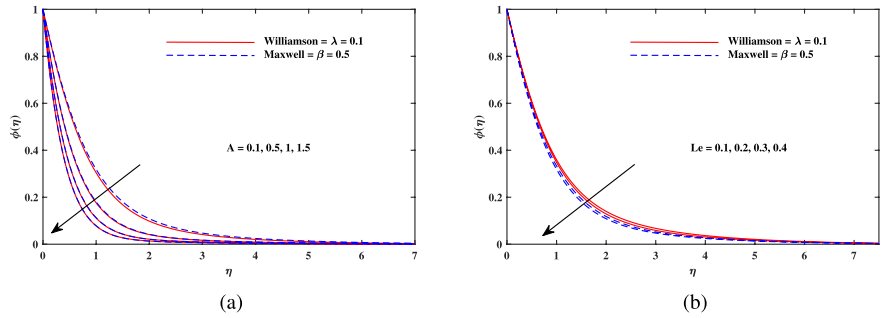

Figure 7. Concentration $\phi(\eta)$ fluctuation with (**a**) A and (**b**) Le.

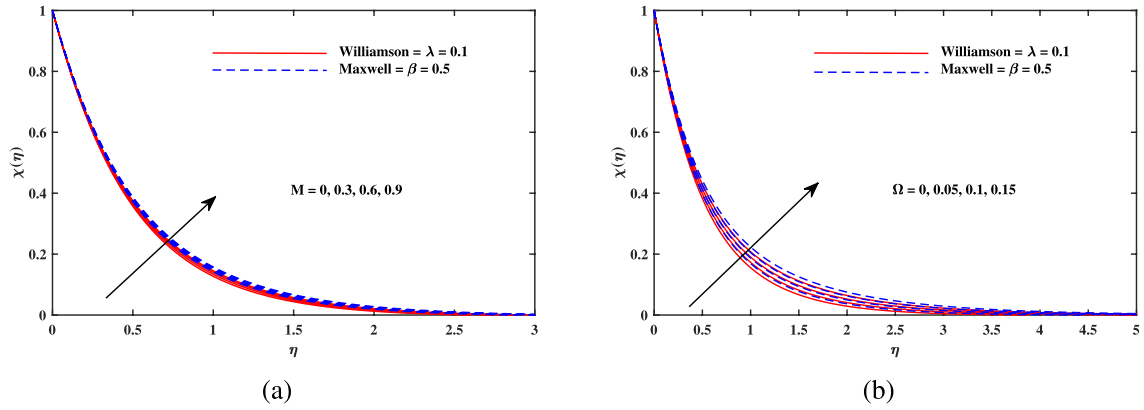

Figure 8. Motile density $\chi(\eta)$ fluctuation with (**a**) M and (**b**) ω.

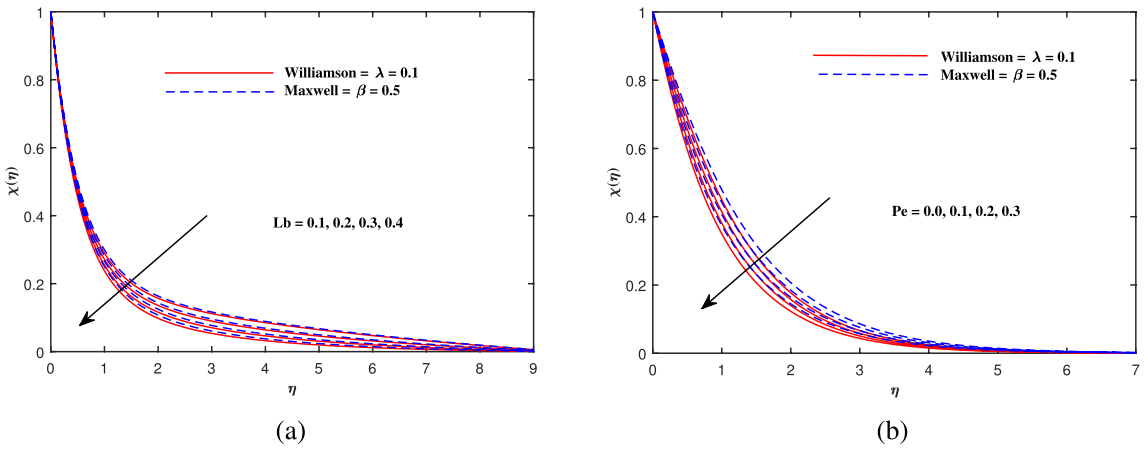

Figure 9. Motile density $\chi(\eta)$ fluctuation with (**a**) Lb and (**b**) Pe.

causes depreciation in diffusivity of microorganisms. The increment in the Peclet number Pe starts a reduction in the motile organisms boundary layer thickness, as well as a decrement in motile density profile $\chi(\eta)$. Moreover, it is clear that larger value of Lb causes a lesser microorganism distribution $\chi(\eta)$.

Conclusion

This article explores the effect of magnetic field, bio-convection and activation energy for Williamson and Maxwell nanofluid on a porous stretched sheet with Cattaneo–Christov diffusion. The main findings of this study are given below:

- Enhancement in magnetic parameter M retards the flow of Williamson fluid and Maxwell fluids.
- Rayleigh number Rb, buoyancy ratio parameter Nr, mixed convection parameter ω, and Kp parameters highly influence on Williamson fluid than Maxwell fluid.

- For temperature profile Cattaneo Christov parameter b, Lewis number Le, and Prandtl number Pr have similar effects. Maxwell fluid is more affected by these parameters than Williamson fluid. On contrary, M and Nc shows opposite behavior for it.
- For concentration profile Williamson fluid is more influenced than Maxwell fluid by M as compared to the other various parameters i.e. Activation energy E, A and Le.
- For motile density profile various parameters i.e. M, microorganisms difference parameter Ω, Lb and Peclet number Pe express more effect for Maxwell fluids as compared to Williamson fluids.
- Skin friction coefficient enhanced for β, M, K_p, Nr and Rb while decrease down for λ and ω.
- Nusselt number reduces when uplifting the parameter Nc, while it increases for Pr, Nbt, and b.
- Sherwood number increases for Sc, A, δ and n while it reduces when uplifting the parameter E.
- Motile density number increases for Lb, Ω and Pe.

Future direction

These results can be further modified and improved for flow of hybrid nanofluids with the implementation of finite element or finite difference discretization.

Received: 18 June 2021; Accepted: 22 December 2021
Published online: 07 January 2022

References

1. Abro, K. A., Soomro, M., Atangana, A. & Gómez-Aguilar, J. Thermophysical properties of Maxwell nanofluids via fractional derivatives with regular kernel. *J. Therm. Anal. Calorim.* **1**, 1–11 (2020).
2. Sharma, R., Hussain, S., Raju, C., Seth, G. & Chamkha, A. J. Study of graphene Maxwell nanofluid flow past a linearly stretched sheet: A numerical and statistical approach. *Chin. J. Phys.* **68**, 671–683 (2020).
3. Ramesh, K. *et al.* Bioconvection assessment in Maxwell nanofluid configured by a riga surface with nonlinear thermal radiation and activation energy. *Surf. Interfaces* **21**, 100749 (2020).
4. Ahmed, J., Khan, M. & Ahmad, L. Radiative heat flux effect in flow of Maxwell nanofluid over a spiraling disk with chemically reaction. *Physica A* **551**, 123948 (2020).
5. Hussain, S. M., Sharma, R., Mishra, M. R. & Alrashidy, S. S. Hydromagnetic dissipative and radiative graphene Maxwell nanofluid flow past a stretched sheet-numerical and statistical analysis. *Mathematics* **8**, 1929 (2020).
6. Jawad, M., Saeed, A. & Gul, T. Entropy generation for mhd Maxwell nanofluid flow past a porous and stretching surface with Dufour and Soret effects. *Braz. J. Phys.* **51**, 469–480 (2021).
7. Williamson, R. V. The flow of pseudoplastic materials. *Ind. Eng. Chem.* **21**, 1108–1111 (1929).
8. Dapra, I. & Scarpi, G. Perturbation solution for pulsatile flow of a non-Newtonian Williamson fluid in a rock fracture. *Int. J. Rock Mech. Mining Sci.* **44**, 271–278 (2007).
9. Nadeem, S., Hussain, S. & Lee, C. Flow of a Williamson fluid over a stretching sheet. *Braz. J. Chem. Eng.* **30**, 619–625 (2013).
10. Haq, F., Kadry, S., Chu, Y.-M., Khan, M. & Khan, M. I. Modeling and theoretical analysis of gyrotactic microorganisms in radiated nanomaterial Williamson fluid with activation energy. *J. Mater. Res. Technol.* **9**, 10468–10477 (2020).
11. Rashid, M., Ansar, K. & Nadeem, S. Effects of induced magnetic field for peristaltic flow of Williamson fluid in a curved channel. *Physica A* **1**, 123979 (2020).
12. Habib, U., Abdal, S., Siddique, I. & Ali, R. A comparative study on micropolar, Williamson, Maxwell nanofluids flow due to a stretching surface in the presence of bioconvection, double diffusion and activation energy. *Int. Commun. Heat Mass Transf.* **127**, 105551 (2021).
13. Waqas, M. *et al.* Interaction of heat generation in nonlinear mixed/forced convective flow of Williamson fluid flow subject to generalized Fourier's and fick's concept. *J. Mater. Res. Technol.* **9**, 11080–11086 (2020).
14. Noreen, S., Waheed, S., Lu, D. & Hussanan, A. Heat measures in performance of electro-osmotic flow of Williamson fluid in micro-channel. *Alexandria Eng. J.* **1**, 10 (2020).
15. Tuz Zohra, F., Uddin, M. J., Basir, M. F. & Ismail, A. I. M. Magnetohydrodynamic bio-nano-convective slip flow with Stefan blowing effects over a rotating disc. *Proc. Inst. Mech. Eng. N* **234**, 83–97 (2020).
16. Sharif, H. *et al.* Energy effects on mhd flow of Eyring's nanofluid containing motile microorganism. *Adv. Concret. Construct.* **10**, 357–367 (2020).
17. Sharma, R. P. & Mishra, S. Combined effects of free convection and chemical reaction with heat-mass flux conditions: A semianalytical technique. *Pramana* **93**, 1–9 (2019).
18. Sharma, R. P. *et al.* Chemical reaction effect on mhd rotating fluid over a vertical plate with variable thermal conductivity: A numerical study. *Indian J. Pure Appl. Phys. (IJPAP)* **56**, 732–740 (2018).
19. Magagula, V. M., Shaw, S. & Kairi, R. R. Double dispersed bioconvective Casson nanofluid fluid flow over a nonlinear convective stretching sheet in suspension of gyrotactic microorganism. *Heat Transf.* **49**, 2449–2471 (2020).
20. Shaw, S., Kameswaran, P., Narayana, M. & Sibanda, P. Bioconvection in a non-darcy porous medium saturated with a nanofluid and oxytactic micro-organisms. *Int. J. Biomath.* **7**, 1450005 (2014).
21. Khan, A. *et al.* Bio-convective micropolar nanofluid flow over thin moving needle subject to Arrhenius activation energy, viscous dissipation and binary chemical reaction. *Case Stud. Therm. Eng.* **25**, 100989 (2021).
22. Choi, S. U. & Eastman, J. A. Enhancing thermal conductivity of fluids with nanoparticles. Tech. Rep., Argonne National Lab. (1995).
23. Esfe, M. H., Esfandeh, S. & Hosseinizadeh, E. Nanofluid flooding for enhanced oil recovery in a heterogeneous two-dimensional anticline geometry. *Int. Commun. Heat Mass Transf.* **118**, 104810 (2020).
24. Khader, M. & Sharma, R. P. Evaluating the unsteady mhd micropolar fluid flow past stretching/shirking sheet with heat source and thermal radiation: Implementing fourth order predictor-corrector fdm. *Math. Comput. Simul.* **181**, 333–350 (2021).
25. Verma, A. K., Gautam, A. K., Bhattacharyya, K. & Sharma, R. Existence of boundary layer nanofluid flow through a divergent channel in porous medium with mass suction/injection. *Sādhanā* **46**, 1–10 (2021).
26. Kumaran, G., Sivaraj, R., Prasad, V. R., Beg, O. A. & Sharma, R. P. Finite difference computation of free magneto-convective Powell-Eyring nanofluid flow over a permeable cylinder with variable thermal conductivity. *Phys. Scr.* **96**, 025222 (2020).
27. Sharma, R. P., Raju, M., Makinde, O. D., Reddy, P. & Reddy, P. C. Buoyancy effects on unsteady mhd chemically reacting and rotating fluid flow past a plate in a porous medium. *Defect Diff. Forum* **392**, 1–9 (2019).
28. Jena, S., Mishra, S., Pattnaik, P. & Sharma, R. P. The nanofluid flow between parallel plates and heat transfer in presence of chemical reaction and porous matrix. *Latin Am. Appl. Res.* **50**, 283–289 (2020).

29. Nayak, M. *et al.* 3d bioconvective multiple slip flow of chemically reactive Casson nanofluid with gyrotactic micro-organisms. *Heat Transf. Asian Res.* **49**, 135–153 (2020).
30. Saranya, S., Ragupathi, P., Ganga, B., Sharma, R. & Hakeem, A. A. Non-linear radiation effects on magnetic/non-magnetic nanoparticles with different base fluids over a flat plate. *Adv. Powder Technol.* **29**, 1977–1990 (2018).
31. Kairi, R. R., Shaw, S., Roy, S. & Raut, S. Thermosolutal marangoni impact on bioconvection in suspension of gyrotactic microorganisms over an inclined stretching sheet. *J. Heat Transf.* **143**, 031201 (2021).
32. Sharma, R. P. *et al.* Time-dependent oscillatory mhd flow over a porous vertical sheet with heat source and chemical reaction effects. *Indian J. Pure Appl. Phys. (IJPAP)* **58**, 877–884 (2020).
33. Ali, B., Ali, L., Abdal, S. & Asjad, M. I. Significance of Brownian motion and thermophoresis influence on dynamics of Reiner–Rivlin fluid over a disk with non-Fourier heat flux theory and gyrotactic microorganisms: A numerical approach. *Phys. Scr.* **96**, 094001 (2021).
34. Yahya, A. U. *et al.* Thermal characteristics for the flow of Williamson hybrid nanofluid (mos2+ zno) based with engine oil over a streched sheet. *Case Stud. Therm. Eng.* **26**, 101196 (2021).
35. Habib, D. *et al.* On the role of bioconvection and activation energy for time dependent nanofluid slip transpiration due to extending domain in the presence of electric and magnetic fields. *Ain Shams Eng. J.* **1**, 10 (2021).
36. Ahmad, F. *et al.* The improved thermal efficiency of Maxwell hybrid nanofluid comprising of graphene oxide plus silver/kerosene oil over stretching sheet. *Case Stud. Therm. Eng.* **2**, 101257 (2021).
37. Rasool, G., Chamkha, A. J., Muhammad, T., Shafiq, A. & Khan, I. Darcy-Forchheimer relation in Casson type mhd nanofluid flow over non-linear stretching surface. *Propul. Power Res.* **9**, 159–168 (2020).
38. Ahmad, F. *et al.* Mhd thin film flow of the Oldroyd-b fluid together with bioconvection and activation energy. *Case Stud. Therm. Eng.* **27**, 101218 (2021).
39. Gul, T., Ahmed, Z., Jawad, M., Saeed, A. & Alghamdi, W. Bio-convectional nanofluid flow due to the thermophoresis and gyrotactic microorganism between the gap of a disk and cone. *Braz. J. Phys.* **51**, 687–697 (2021).
40. Gul, T. *et al.* Magneto hydrodynamic and dissipated nanofluid flow over an unsteady turning disk. *Adv. Mech. Eng.* **13**, 16878140211034392 (2021).
41. Abbas, Z. *et al.* Mhd boundary layer flow and heat transfer of nanofluid over a vertical stretching sheet in the presence of a heat source. *Sci. Inquiry Rev.* **3**, 60–73 (2019).
42. Ali, L., Liu, X., Ali, B., Mujeed, S. & Abdal, S. Finite element analysis of thermo-diffusion and multi-slip effects on mhd unsteady flow of Casson nano-fluid over a shrinking/stretching sheet with radiation and heat source. *Appl. Sci.* **9**, 5217 (2019).
43. Krishnamurthy, M., Prasannakumara, B., Gireesha, B. & Gorla, R. S. R. Effect of chemical reaction on mhd boundary layer flow and melting heat transfer of Williamson nanofluid in porous medium. *Eng. Sci. Technol.* **19**, 53–61 (2016).
44. Abdal, S. *et al.* Implications of bioconvection and activation energy on Reiner–Rivlin nanofluid transportation over a disk in rotation with partial slip. *Chin. J. Phys.* **73**, 672–683 (2021).
45. Habib, D., Abdal, S., Ali, R., Baleanu, D. & Siddique, I. On bioconvection and mass transpiration of micropolar nanofluid dynamics due to an extending surface in existence of thermal radiations. *Case Stud. Therm. Eng.* **27**, 101239 (2021).
46. Abdal, S. *et al.* Radiation and multiple slip effects on magnetohydrodynamic bioconvection flow of micropolar based nanofluid over a stretching surface. *Appl. Sci.* **11**, 5136 (2021).
47. Abdal, S., Hussain, S., Siddique, I., Ahmadian, A. & Ferrara, M. On solution existence of mhd Casson nanofluid transportation across an extending cylinder through porous media and evaluation of priori bounds. *Sci. Rep.* **11**, 1–16 (2021).
48. Nadeem, S. & Hussain, S. Flow and heat transfer analysis of Williamson nanofluid. *Appl. Nanosci.* **4**, 1005–1012 (2014).
49. Khan, W. & Pop, I. Boundary-layer flow of a nanofluid past a stretching sheet. *Int. J. Heat Mass Transf.* **53**, 2477–2483 (2010).
50. Gorla, R. S. R. & Sidawi, I. Free convection on a vertical stretching surface with suction and blowing. *Appl. Sci. Res.* **52**, 247–257 (1994).

Acknowledgement

The authors would like to acknowledge and express their gratitude to the United Arab Emirates University, Al Ain, UAE for providing financial support with Grant No. 12S086.

Author contributions

S.A.: Conceptualization, methodology, design; I.S.: Data curation, writing—original draft preparation. D.A.and Q.M.: Supervision and validation of data—reviewing original draft. S.H.: Supervision, Reviewing and editingthe final version and validation of data.

Competing interests

The authors declare no competing interests.

Additional information

Correspondence and requests for materials should be addressed to Q.A.-M.

Reprints and permissions information is available at www.nature.com/reprints.

Publisher's note Springer Nature remains neutral with regard to jurisdictional claims in published maps and institutional affiliations.